Continental Shelf Research
May 2022, Volume 240, Pages 104698 (14p.)
https://doi.org/10.1016/j.csr.2022.104698
https://archimer.ifremer.fr/doc/00755/86662/

An investigation of sea level and circulation response during a coastal trapped wave event on the Eastern Agulhas Bank, South Africa

Bailey Dylan F. [1, 2, *], Hermes Juliet [2, 3], Penven Pierrick [4], Bornman Thomas G. [2, 3], Goschen Wayne [3]

[1] Bayworld, Port Elizabeth Museum, Port Elizabeth, South Africa
[2] South African Environmental Observation Network, Elwandle and Egagasini Nodes, South Africa
[3] Institute for Coastal and Marine Research, Nelson Mandela University, Port Elizabeth, South Africa
[4] University of Brest, CNRS, IRD, Ifremer, Laboratoire d'Océanographie Physique et Spatiale, IUEM, France

* Corresponding author : Dylan F. Bailey, email address : dylan.bailey@bayworldoceanarium.com

Abstract :

An investigation into the ocean response to a protracted (>48 h) strong south-westerly wind event averaging 9.6 m/s on the eastern Agulhas Bank, South Africa, using in situ instrument data from Algoa Bay and a high resolution (dx ~1 km) ROMS ocean model, is presented. A coastal trapped wave (CTW) was shown to be associated with the event, the peak amplitude of which increased as it travelled eastward through the domain. Alongshore current reversals to the full depth were seen in both the model and two acoustic doppler current profiler (ADCP) moorings (30 m bottom depth) as the CTW traversed the study domain, with strong currents exceeding 1 m/s developing directly to the south of Cape St Francis and Cape Recife at the peak of the wind event within the model. In a model run with wind forcing removed, the effects of remote wind forcing were shown to be a significant contributor to local circulation during strong wind events, suggesting that an estimated 61% of the total eastward transport of shelf water over the entire period of the event was due to remote forcing. In the no-wind model, a short lived anticyclonic rotating feature forms in the lee of Cape Recife in Algoa Bay shortly after the peak of the CTW, in contrast to the reference model, where instead a broad anticyclonic flow throughout the bay establishes.

Highlights

► The Regional Oceanographic Modelling System has predictive skill in reproducing coastal trapped wave events along the south coast of South Africa. ► Sudden alongshore current reversals are seen to full depth in the model and ADCP mooring data. ► The model shows very strong eastward currents develop off Cape St Francis and Cape Recife. ► The model shows very large volume displacement caused by the CTW, which carries most of the energy from remote wind forcing to the west of Oyster Bay

Keywords : Coastal Trapped Wave, Regional Ocean Modelling System, Wind Event, Agulhas Bank, Algoa Bay

1. Introduction

In this study, the Regional Ocean Modelling System (ROMS) is used to examine circulation patterns and sea level changes during a protracted south-westerly wind event with an average of 9.6 m/s that lasted approximately 58 hours on the eastern Agulhas Bank off the south coast of South Africa. A detailed analysis is made of the effects of the wind event passing through the two bays on this portion of the South African coastline, namely St Francis Bay and Algoa Bay, and the adjacent shelf using a combination of a reference run and a no-wind run together with *in situ* instrument mooring data.

Algoa Bay is a large log-spiral shaped bay located on the south eastern coast of South Africa facing into the Southwest Indian Ocean. The bay is relatively shallow, less than 70 m deep, with the depth of the adjacent shelf reaching 150 m near the shelf break, which lies about 50 km south-east of Cape Recife (Bremner 1983). A study involving ship transects and vertical profiling instruments by Goschen & Schumann (1988) demonstrated that wind and the Agulhas Current (AC) are the primary driving forces behind circulation patterns within Algoa Bay. In general, currents in the bay tend to align to the direction of the prevailing wind, modified by the topography and the shape of the coast. This typically holds true for circulation over the shelf away from the influence of the AC. In the shallow western sector of the bay, Schumann et al. (2005) demonstrated that generally, wind was important in surface water movement and setting up of pressure gradients resulting in the generation of geostrophic currents. While surface currents tend to follow prevailing winds across the wider reaches of the bay, deeper offshore waters often flow in a more south to south-westward direction. While the exact mechanism for this deeper flow is yet to be described, it is possibly linked to entrainment of shelf water by the AC in a similar manner described by Swart and Largier (1987). In the north-eastern sector of the bay, Roberts (2010) and Pattrick et al. (2013) found that there is a strong correlation between currents and prevailing

wind directions, even in the deeper layers within 2km of the coast, coupled with overall stronger current velocities to that of the western sector. These differences are likely due to topographic influences such as shoreline orientation to prevailing wind directions in the different regions of the bay. Pattrick et al. (2013) showed that current structures in the shallow nearshore area of north-eastern Algoa Bay to be complex, with the dominant flow towards the east.

Eastward propagating wind systems along the south coast of South Africa can induce shelf waves through resonance, which then travel perpendicular to the coastline in an eastward direction in near-resonance with these wind systems (Gill and Schumann 1974). Should the forcing of these waves be initiated simultaneously to the alongshore wind stress creating an onshore-offshore transport within the Ekman layer, a compensating offshore-onshore flow is created at a greater depth as a result of mass conservation (Brink 1991). The local relative vorticity changes as the flow crosses isobaths, and since this process expresses itself largely in terms of alongshore velocity, interaction with any alongshore variability will result in wave propagation. The resulting coastally-attached sub-inertial continental shelf wave then propagates along the coast on its left-hand side due to the conservation of potential vorticity (Maiwa et al. 2010) and is then considered a coastal trapped wave (CTW). An assessment of air pressure and tide level recorders by Schumann (1983) provides further evidence on the existence of CTW off the south coast of South Africa, which typically occur as barotropic shelf waves with periods within the weather band of between 3 and 20 days and phase propagation speeds anywhere between 4.4 to over 9 m/s (Schumann and Brink 1990). Large CTW can have profound, although short lived, effects on the regional ocean state and can be a considerable contributor to near shore variability (e.g. Tilney et al. 1996, Schumann 1999). Circulation over the shelf and in St Francis Bay and Algoa Bay can experience periodic barotropic changes due to the passage of CTW. Data analysed from Acoustic Current Doppler Profilers (ADCP), deployed by Goschen et al. (2012) off Woody Cape in the north-eastern sector of Algoa Bay, show that currents here are influenced by CTW passing through this region, causing periodic reversals in current flow. In the western sector of the bay, however, although CTW are present, it appears that there is little influence on the currents in this region (Schumann et al. 2005). It is believed that this is due to the abrupt headland at the south-western corner, coupled with the change in the coastal boundary from the southern coast to

the bay. The waves eventually dissipate as they travel eastward along the narrowing shelf and interact with the south-westward flowing AC (Brink 1990, 2006).

2. Data and Methods

2.1 Study Area

The region of focus is the eastern Agulhas Bank, found on the south-eastern portion of the southern African continental shelf (Figure 1). The shelf here has an average depth of 120 m and progressively narrows to the north-east, from 50 km off Cape St Francis to 34 km off Port Alfred (measured from the coast to the 200 m isobath), bounded by a coastline to the north and a steep shelf break to the south that descends rapidly to beyond 1000 m depth. The shelf break is flanked by the Agulhas Current (AC), a major western boundary current that follows the continental shelf break on the east coast of southern Africa with a typical width of 70-90 km, a depth of 2300 m, and a surface core velocity often exceeding 2.5 m/s (Roberts et al. 2010), with a mean southward transport of between 77 and 84 Sv (Beal et al. 2015). Two large log-spiral bays are found near 34°S, Algoa Bay and St Francis Bay. The domain of this study extends from Oyster Bay to north of Port Alfred, outlined in Figure 1b.

2.2 Numerical Model

The Regional Ocean Modelling System (ROMS), a split-explicit, terrain following regional oceanographic model using a third-order, upstream-biased advection scheme (Shchepetkin and McWilliams 2005) was used for the numerical simulations. To resolve fine scale coastal circulation while giving consideration to larger mesoscale dynamics, a multi-nested downscaling technique was employed to resolve disparities in spatial and temporal scales. A one-way, offline method of model nesting to finer scale was used without feedback from the child grid solutions (Penven et al. 2006b). Consideration of the open boundary condition (OBC) configuration was given to the approaches described by Penven et al. (2006a), Mason et al. (2010) and Marchesiello et al. (2001) for offline regional ocean model nesting. For the ROMS configuration described here, prognostic variables were connected to the external conditions in the open boundary configurations using Orlanksi active radiation schemes for the baroclinic mode (for both temperature and salinity), and modified Flather-type characteristic radiation scheme for the barotropic mode. This was coupled with a

nudging scheme, as described by Mason et al. (2010), to ensure that external information was adequately incorporated through the boundaries. A total of four regional model domains, a parent and three child nests, were defined on an Arakawa-C Mercator grid, hereafter referred to as SAnL0, SAnL1, SAnL2, and SAnL3 respectively (Figure 1). Child grids were nested in a one-way and offline configuration using a downscaling factor of 3. Domain specific configurations, including time frames for surface forcing, lateral boundary forcing and spin up are summarized in Table 1. SAnL0 was the parent grid, providing lateral climatological boundary conditions for the first nest SAnL1. Lateral boundary conditions for SAnL2 and SAnL3 were then extrapolated from the outputs of the prior nest. All grids and forcing files were created using ROMSTOOLS (https://www.croco-ocean.org/download/roms_agrif-project/), a toolbox of Matlab scripts and datasets that aid in the configuration of grids and production of forcing files for ROMS. Additional Matlab code was used from the ROMS Numerical Toolbox (http://oces.us/RNT/) to produce the offline lateral boundary conditions between nested grids. The parent domain, SAnL0, uses a modified SAfE configuration (Penven et al. 2006a), where the surface is forced using an interannual atmospheric dataset and the lateral boundary conditions are forced using the World Ocean Atlas 2009 (WOA09) monthly climatology. This configuration was chosen as to reduce the introduction of biases that would have occurred if lateral boundary forcing from an inter-annual global ocean model was used. A full evaluation was carried out to ensure that the parent SAnL0 model was of a suitable size and resolution to resolve the most important of the basin scale processes at the correct time scales for the subsequent nests (Bailey 2020).

A surface forcing atmospheric dataset with hourly wind variables was chosen in order to resolve fine temporal scale coastal ocean circulation as accurately as possible (Cucco et al. 2019). The NCEP Climate Forecast System version 2 (CFSv2) (Saha et al. 2014) provided historical hourly timeseries analysis over the required time period on a 0.205° by 0.205° global grid. The 30 arc-second GEBCO_2014 gridded dataset (version 20150318, www.gebco.net) provided the bathymetric data for all domains. This was bilinearly interpolated onto the grid and smoothed with an r-factor of 0.2 to reduce pressure gradient errors (Haidvogel and Beckmann 1999). All model domains had 42 vertical σ-coordinate levels with surface and bottom grid stretching factors of θ_s = 6 and θ_b = 0, respectively. Models were run in a free slip configuration using a

split and rotated 3rd order upstream biased advection scheme (Marchesiello et al. 2009). The integration period was five years, spanning from 1 January 2011 to 31 December 2015, with averaged outputs of temperature, salinity, and momentum (sampling periods shown on Table 1). Models were spun up by repeating the 2011 forcing year as many times as needed to obtain statistical equilibrium (shown in Table 1).

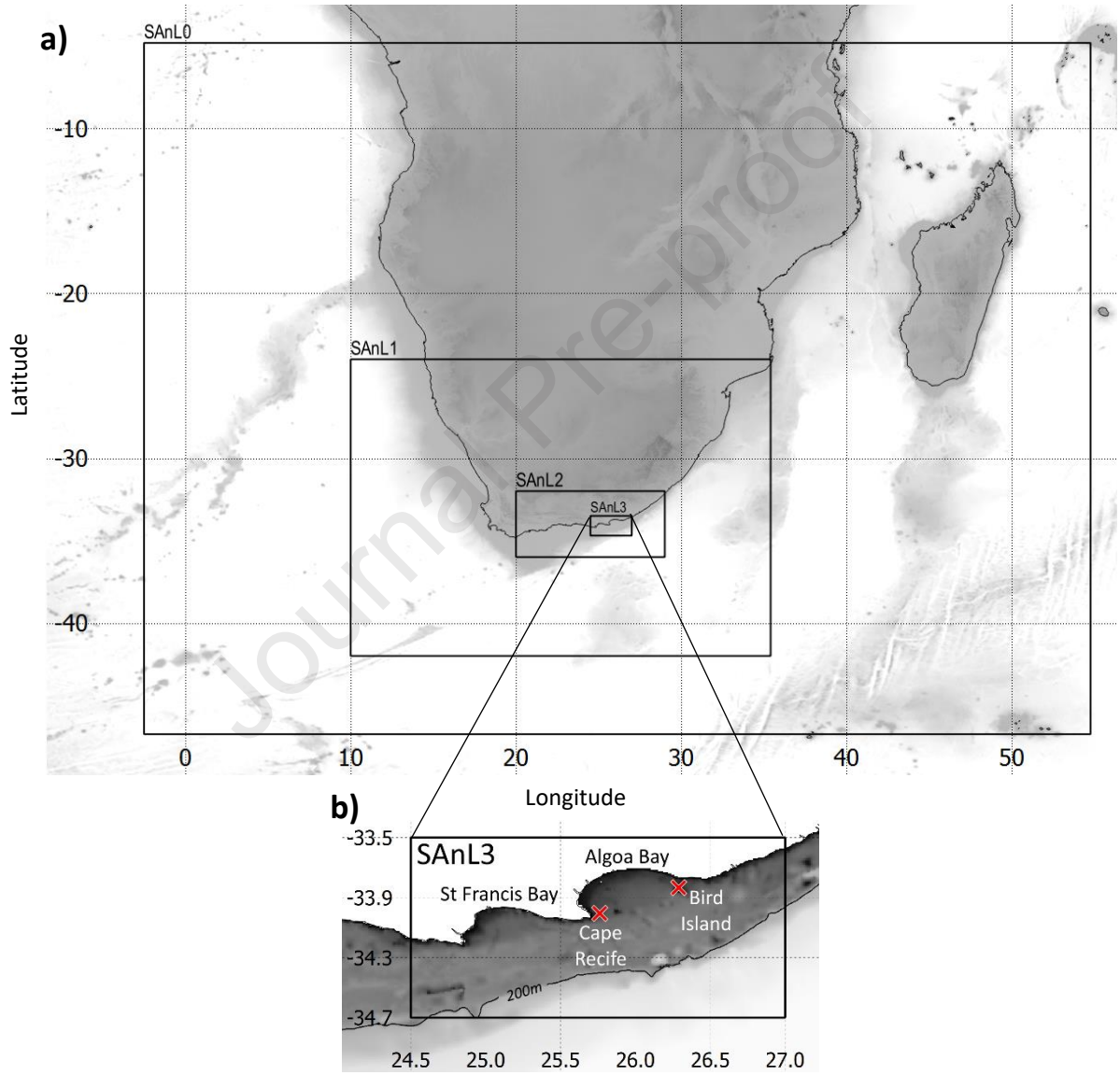

Figure 1 (a) Relative position of the model domains, outlined by solid black lines, with respect to the sub-Saharan African and Madagascan continent. (b) Extents of SAnL3 model domain from Oyster Bay to north of Port Alfred, encompassing St Francis Bay and Algoa Bay, used in this study, with the locations of the SAEON ADCP and UTR moorings at Cape Recife and Bird Island. Latitude and longitude in decimal degrees. Shelf to the 200m isobath denoted by dark shaded area, with 200m isobath shown in (b).

173 *Table 1 Nested domain configurations for ROMS*

	SAnL0	SAnL1	SAnL2	SAnL3
Domain Extents	2.5° W - 54.75° E; 4.8° S - 46.75° S	10.0° E - 35.4° E; 24.0° S - 42.0° S	20.0° E - 29.0° E; 32.0° S - 36.0° S	24.5° E - 26.5° E; 33.7° S - 34.7° S
Domain Resolution	1/4° (~28km)	1/12° (~9 km)	1/36° (~3 km)	1/108° (~1km)
Surface Forcing	NCEP CFSv2	NCEP CFSv2	NCEP CFSv2	NCEP CFSv2
Bulk Flux Forcing Time	6 h	6 h	6 h	6 h
Surface Wind Stress	6 h	6 h	1 h	1 h
Lateral Boundary Forcing	WOA05	SAnL0	SAnL1	SAnL2
Lateral Boundary Time	Monthly	Daily	8 h	3 h
Tides Enabled	No	No	No	Yes
Spin Up Period	5 years	3 years	1 year	1 year
Output Time	Daily	8 h	3 h	3 h

174

175 ### *2.3 Observation Data*

176 *In situ* current data was obtained from the South African Environmental Observation
177 Network (SAEON) Acoustic Doppler Current Profiler (ADCP) instrument moorings
178 located at Cape Recife (Figure 2: A1) and Bird Island (Figure 2: A2) on the eastern
179 and western extents of Algoa Bay respectively. Sea level data was obtained from the
180 South African National Hydrographers Office (SANHO) Tide Recorder located at the
181 Port Elizabeth Harbour in Algoa Bay (Figure 2: D1), as well as Port Nolloth, Cape
182 Town, Mossel Bay, Knysna, and East London. Weather data was obtained from the
183 South African Weather Services (SAWS) Automatic Weather Stations (AWS) at Cape
184 Agulhas, Plettenberg Bay, Port Elizabeth, Coega, Bird Island, Port Alfred and East
185 London (Figure 4).

186 ### *2.4 Identification of events for case study*

187 Only a few strong south-westerly wind events occurred in the time period of the model
188 that provided optimal conditions for an assessment. Ideally, the Agulhas Current (AC)
189 should not be in a meandering state and be free of cyclonic eddy activity (eg.
190 Lutjeharms and Roberts 1988, Schumann and van Heerden 1988, Lutjeharms et al.
191 2003a, 2003b) (confirmed by visual inspection of sea surface temperature (SST)) in
192 both the numerical model and *in situ* environment, and ADCP and Tide Recorder data
193 should be available for that time. Considering these requirements, only a single wind
194 event, occurring between 17 September 2014 and 20 September 2014 (Figure 3),

presented itself. It was also the only significant south-westerly wind event to occur for that month.

2.5 Sea level, alongshore currents, and along-shelf transport assessment

Four key locations in the model located within 6km of the shoreline (Figure 2 red stars: south of Cape St Francis (B1) (65 m depth), Cape Recife (B2) (55 m depth), and Bird Island (B3) (35 m depth), and southeast of Port Alfred (B4) (30 m depth)) were used to assess sea level and alongshore currents during the event. Along-shelf volume transport (assessed by depth-integration of flow along a transect) was measured between Cape Recife and 10km inshore of the mean position of the AC inshore front to reduce interference from any submesoscale (O(<10 km)) frontal variability (Figure 2 dashed line: C1) (Lutjeharms et al. 1989, Krug et al. 2017, Tedesco et al. 2019).

The influence of remote forcing on the circulation on the shelf and bays during the event was assessed by comparing the SAnL3 reference model with a modified SAnL3 model run where all surface wind forcing was removed while maintaining advective surface heat fluxes. Shelf waves and edge waves (CTW) and currents were free to pass through the domain in this configuration, but with no further input of kinetic energy from local wind forcing.

Unless otherwise stated, all sea level plots were filtered using a Lanczos filter with a quarter-power point of 0.031 cycles per hour to remove tides, and all wind plots were filtered using a Lanczos filter with a quarter-power point of 0.03509 cycles per hour. Wind stick plots were averaged to three hours to match *in situ* and model time steps. Sea level correction along the south coast was done for Port Elizabeth, using air pressure (Gaspar and Ponte 1997) from the AWS at the Port Elizabeth Airport, and Mossel Bay, using pressure from George Airport, to estimate propagation speeds of the CTW. Depth-integrated (barotropic) currents were calculated by weighted averaging of current velocities for each depth bin height (0.2 m – 0.3 m) in the ADCP data and each grid cell height in the numerical model.

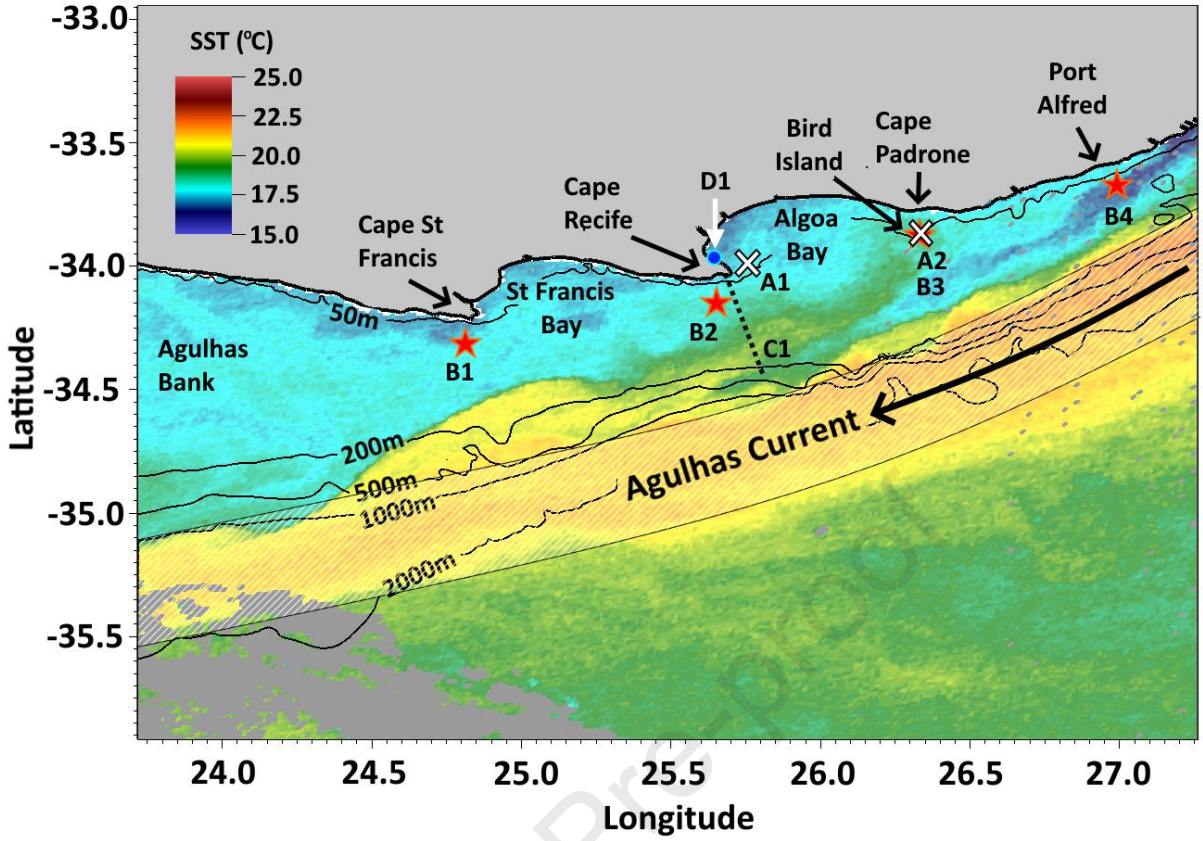

223

224 *Figure 2 MODIS sea surface temperature (SST) image taken on 21 July 2009 with bathymetry overlay*
225 *of the south eastern coast of South Africa off Algoa Bay to illustrate the typical path of the warm (> 21*
226 *°C) Agulhas Current as indicated off the continental shelf margin. White crosses denote locations of*
227 *Cape Recife (A1) and Bird Island (A2) ADCP moorings. Red stars denote locations of the Cape St*
228 *Francis (B1), Cape Recife (B2), Bird Island (B3) and Port Alfred (B4) locations used for current*
229 *assessments in the numerical models. Dashed line denotes transect used for volume transport*
230 *assessment (C1). Location of the SANHO Tide Recorder at the Port Elizabeth Harbour shown by blue*
231 *dot (D1). The Port Elizabeth SAWS weather station at the Port Elizabeth Airport is approximately 3km*
232 *inland of the Port Elizabeth Harbour.*

233

234

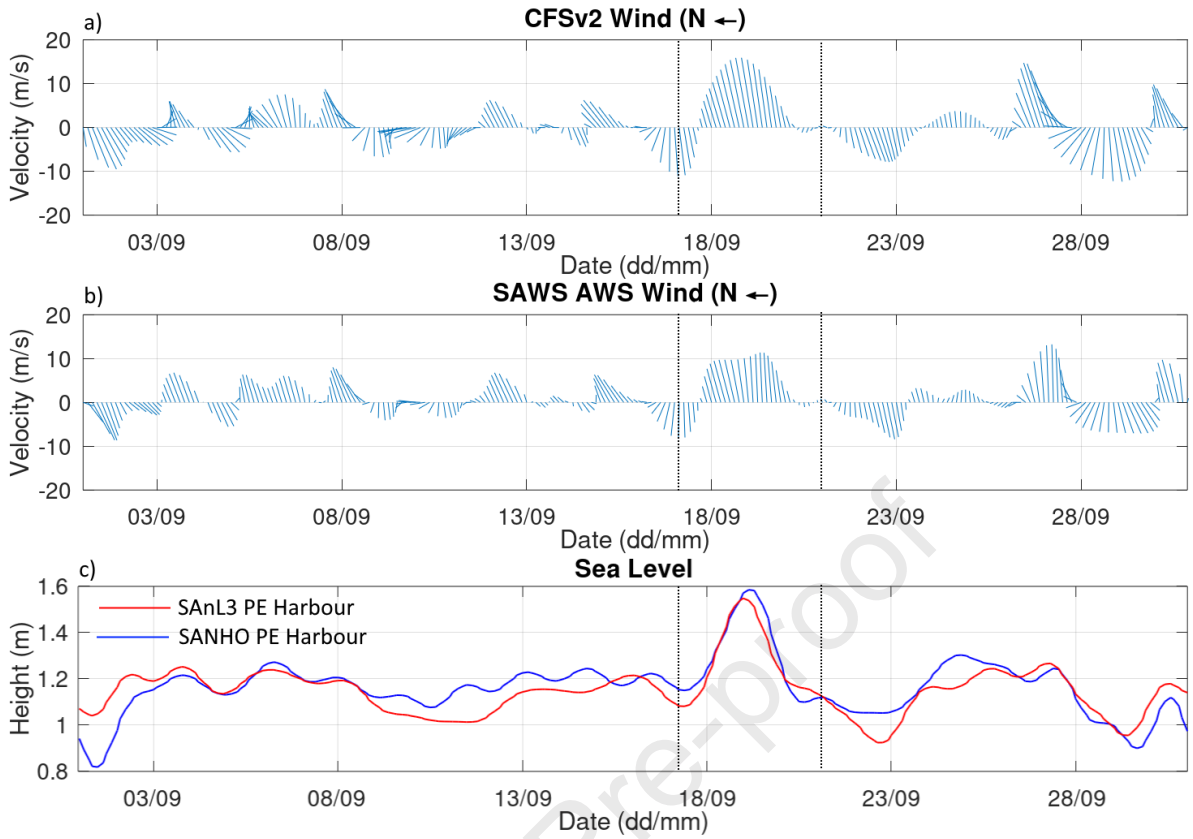

235

236 *Figure 3 (a) Wind plot from the CFSv2 dataset extracted at the SAWS AWS location at the Port*
237 *Elizabeth airport. (b) Wind plot from the SAWS AWS at the Port Elizabeth airport. (c) Uncorrected sea*
238 *surface height from the SANHO tide recorder at the Port Elizabeth (PE) harbour (blue) and the closest*
239 *grid cell in the SAnL3 reference model (red). Dates shown from 1 September 2014 to 31 September*
240 *2014. Coastal trapped wave event between 17 September 2014 and 22 September 2014 highlighted*
241 *with dashed lines. Date lines denote midnight.*

242

3. Results

3.1 Wind and Model Skill Evaluation

Correlation coefficients (*R*) and relative bias in wind velocity between the Automatic Weather Station (AWS) wind data from the South African Weather Service (SAWS) and the closest georeferenced grid cell in the CFSv2 dataset (Figure 4) revealed a good correlation for most stations, with an average R-value of 0.83 ($p<0.05$) (results summarised in Table 2). Relative bias for wind speeds were within 20% for most stations. The relatively poor correlation and high wind bias at the Plettenberg Bay AWS was due in part to large portions of missing readings in the dataset.

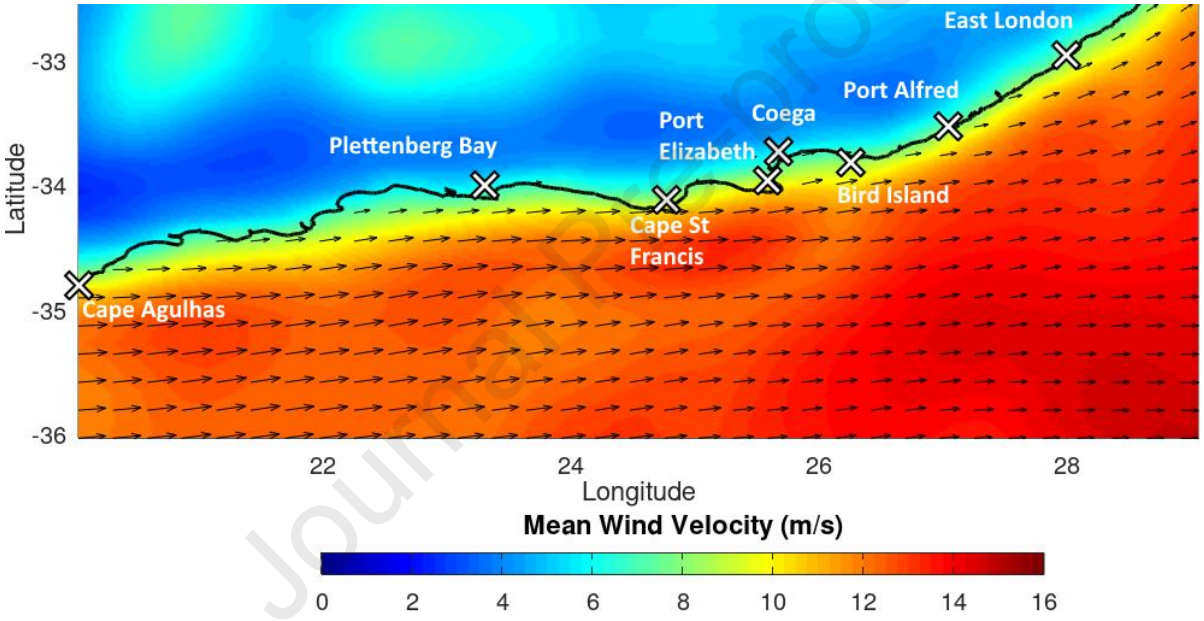

Figure 4 Mean CFSv2 10m wind field for the SAnL2 model domain during the westerly wind event from 12h00 17 September 2014 to 12h00 20 September 2014. Locations of SAWS weather stations used for wind skill assessments shown.

Table 2 Comparative analysis of NCEP CFSv2 10m wind and SAWS AWS wind for the period 1 January 2011 to 31 December 2015. Stations in the SAnL3 study domain highlighted in bold. Relative bias shown as CFSv2 wind velocity over AWS.

AWS Station	Location		Altitude (m)	R (p<0.05)	Relative Bias
	Latitude	Longitude			
Cape Agulhas	-34.8262	20.0131	11	0.91	+ 97 %
Plettenberg Bay	-34.0896	23.3259	138	0.54	+ 69 %
Cape St Francis	-34.2122	24.8357	9	0.78	- 3.5 %
Port Elizabeth	-33.9827	25.6138	60	0.94	+ 18.9 %
Coega	-33.8050	25.6680	46	0.92	+ 10.9 %
Bird Island	-33.8388	26.2861	3	0.9	+ 15 %
Port Alfred	-33.5595	26.8809	84	0.91	+ 46 %
East London	-33.0225	27.8199	149	0.88	+ 6.9 %

Correlation factor, bias and Root-Mean-Square-Error (RMSE) were used along with the cost function χ, the ratio of RMSE against the standard deviation of the observations (Holt et al. 2005), to assess model performance against observations between 1 September 2014 to 31 September 2014 (results summarised in Table 3). For the cost function χ, values less than 1 (RMSE smaller than the standard deviation of the observations) indicate that the predictive skill of the model is acceptable (Holt et al. 2005). Sea surface height had the overall best performance, with comparisons against the SANHO tide level recorder (Figure 5c;Table 3) resulting in an R value ($p<0.05$) of 0.8, a mean bias of 0.013 m (σ 0.015 m) (Mean SSH 1.152 m), and χ of 0.62. Depth-averaged velocities showed less agreement. Zonal (eastward) and meridional (northward) current component velocities for Bird Island (Figure 5a) had a relatively good correlation of 0.74 and 0.72 respectively, with χ indicating a better agreement in the zonal component (0.72) compared to the meridional component (0.88). Cape Recife (Figure 5b) performed the worst with regards to the zonal component velocities, with a correlation of 0.29 and χ of 1.05. The meridional component velocities performed moderately better with a correlation of 0.66 and χ of 0.85. However, as shown in the scatterplot of Figure 5b, a positive bias in the model at higher southward velocities is evident. The site is directly to the east of a major headland, oriented perpendicular to south-westerly winds, with a relatively complex topographic gradient not well represented in the GEBCO topography. As a result, flow patterns during south-westerly winds are complex, leading to a poor representation of

zonal velocities in the model (Figure 7a,c) and likely contributing to the bias in southward meridional velocities.

Table 3 Model skill assessment between observed and modelled depth integrated current velocity and sea surface height from 1 September 2014 to 31 September 2014.

	BIAS	R (p<0.05)	RMSE	X
Cape Recife (A1) Eastward Current (m/s)	0.013	0.29	0.062	1.05
Cape Recife (A1) Northward Current (m/s)	-0.081	0.66	0.180	0.85
Bird Island (A2) Eastward Current (m/s)	-0.071	0.74	0.213	0.72
Bird Island (A2) Northward Current (m/s)	-0.043	0.72	0.093	0.88
Port Elizabeth Harbour (D1) Sea Level (m)	0.013	0.8	0.076	0.62

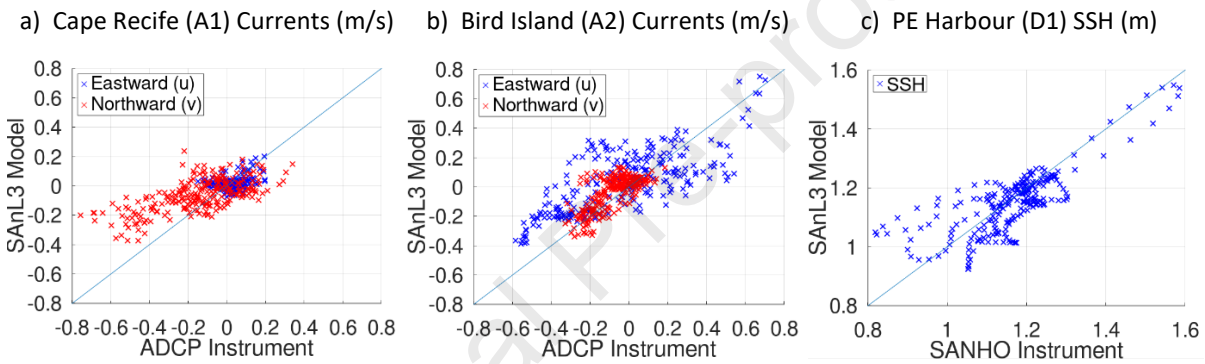

Figure 5 Scatter plots of (a) the SAnL3 model depth integrated currents against SAEON ADCP moorings at Cape Recife (A1) and (b) Bird Island (A2). (c) The SAnL3 model sea surface height (SSH) against the SANHO tide level recorder in the Port Elizabeth Harbour (D1). Plot data from 1 September 2014 to 31 September 2014. Negative values are southward/westward flow.

3.2 The regional ocean response to a large wind event

The south-westerly wind event began during the evening of 17 September 2014 following a north easterly wind event and persisted for a total of 58 hours (2.5 days). Hourly average wind speeds measured at the Port Elizabeth Airport AWS varied between 5.6 m/s and 15.7 m/s, with an average of 9.6 m/s over the entire duration of the event (Figure 3b). The peak wind speed of 15.7 m/s (near gale) occurred on 19 September at 11h00. The wind event was associated with a large fluctuation in sea level with an amplitude of 45 cm measured at the SANHO tide level recorder at the Port Elizabeth Harbour (Figure 3c). The mean water level rose from 1.14 m to 1.59 m over a period of 42 hours, reaching its peak at 04h00 on 19 September 2014, with a similar response observed in the SAnL3 model (Figure 3c). The water level increase was associated with a CTW, which followed the typical anti-clockwise passage of CTW

around southern Africa, first recorded by the Port Nolloth tide gauge on the west coast, increasing in amplitude as the wave travelled along the south coast, and then dissipating near East London on the east coast, as described by Schumann and Brink (1990) and Schumann (2013) (Figure 6a). The wave was associated with a propagating low-pressure system, evident by high zonal wind speeds associated with a large change in air pressure, shown for Mossel Bay and Port Elizabeth in Figure 6b,c,d. This indicates that the wave was initiated and propagated in resonance with the system as it travelled along the coast. The peaks in corrected sea level records between Mossel Bay and Port Elizabeth occurred exactly 12 hours apart (Figure 6b), which indicates a propagation speed of the wave along the south coast, measured peak to peak, of approximately 7.5 m/s. Surprisingly, this perfectly matches the propagation speed calculated by Schumann and Brink (1990).

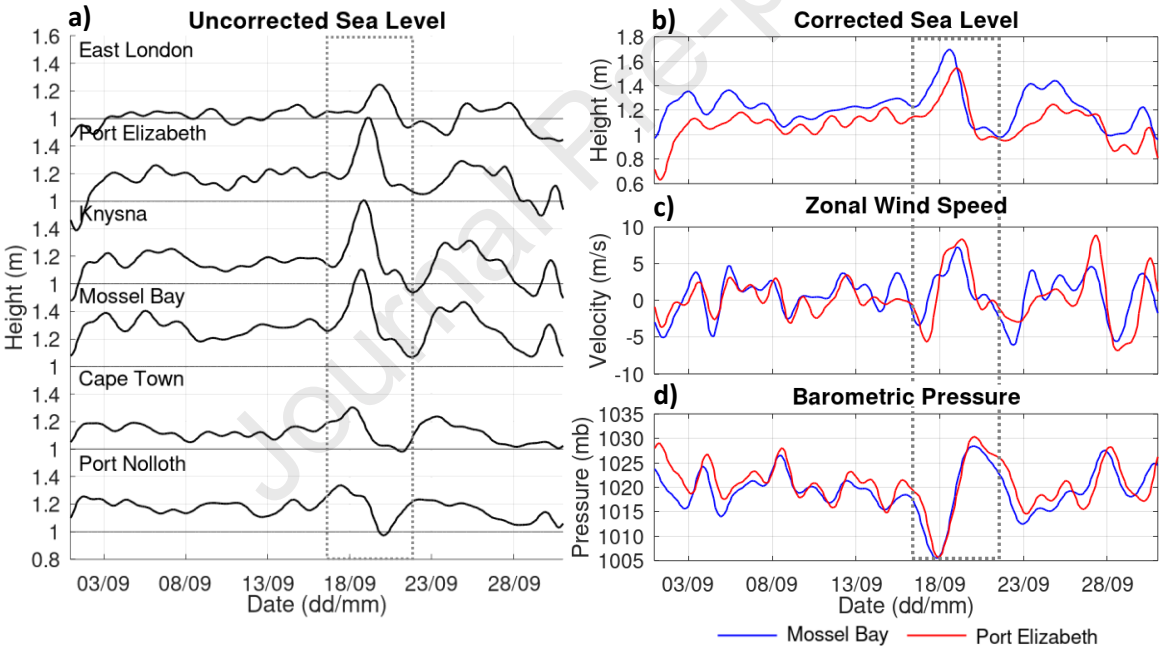

Figure 6 (a) Uncorrected SANHO tide level records from Port Nolloth on the west coast of South Africa (tbottom) to East London on the east coast (top). (b) Pressure corrected sea level, (c) zonal wind speed (positive eastward) and (d) barometric pressure for Mossel Bay (blue) and Port Elizabeth (red). Dates shown from 1 September 2014 to 31 September 2014. Coastal trapped wave event between 17 September 2014 and 22 September 2014 highlighted with grey dashed box.

The ocean response to the wind event was captured by the SAEON ADCP moorings at Cape Recife and Bird Island. The alongshore current at Cape Recife (meridional rotated 23° anti-clockwise), which is usually dominated by southward flow (Figure 7a), underwent a barotropic reversal shortly after the arrival of the leading edge of the wave at 12h00 on 17 September 2014 (Figure 8b,d). The northward flow lasted for approximately 23 hours before mostly resuming to a southward flow just prior to the

peak of the wave. At the Bird Island mooring, the alongshore current (zonal rotated 20° clockwise, according to the isobath contours) saw a relatively quick barotropic current reversal that took place from the onset of the wave, lasting approximately 60 hours (Figure 8b,e). The current reversal occurred within 1 hour to the arrival of the south-westerly wind event, although it was a full 2 hours ahead of the current reversal seen at the Cape Recife mooring. The wave and subsequent response in alongshore current was well represented in the numerical model (Figure 8f,g,h). An approximate three-hour delay in the barotropic response in alongshore currents at Bird Island, compared to the ADCP mooring, was noted (Figure 8e,j). Maximum depth integrated current speeds near the peak of the wave were exceptionally close between the ADCP observations and the numerical model. At Bird Island, eastward flows peaked at 0.77 m/s and 0.72 m/s for the ADCP and SAnL3 model respectively (Figure 8c,h: green plot). At Cape Recife, northward flows peaked at 0.17 m/s and 0.16 m/s for the ADCP and SAnL3 model respectively (Figure 8c,h: red plot).

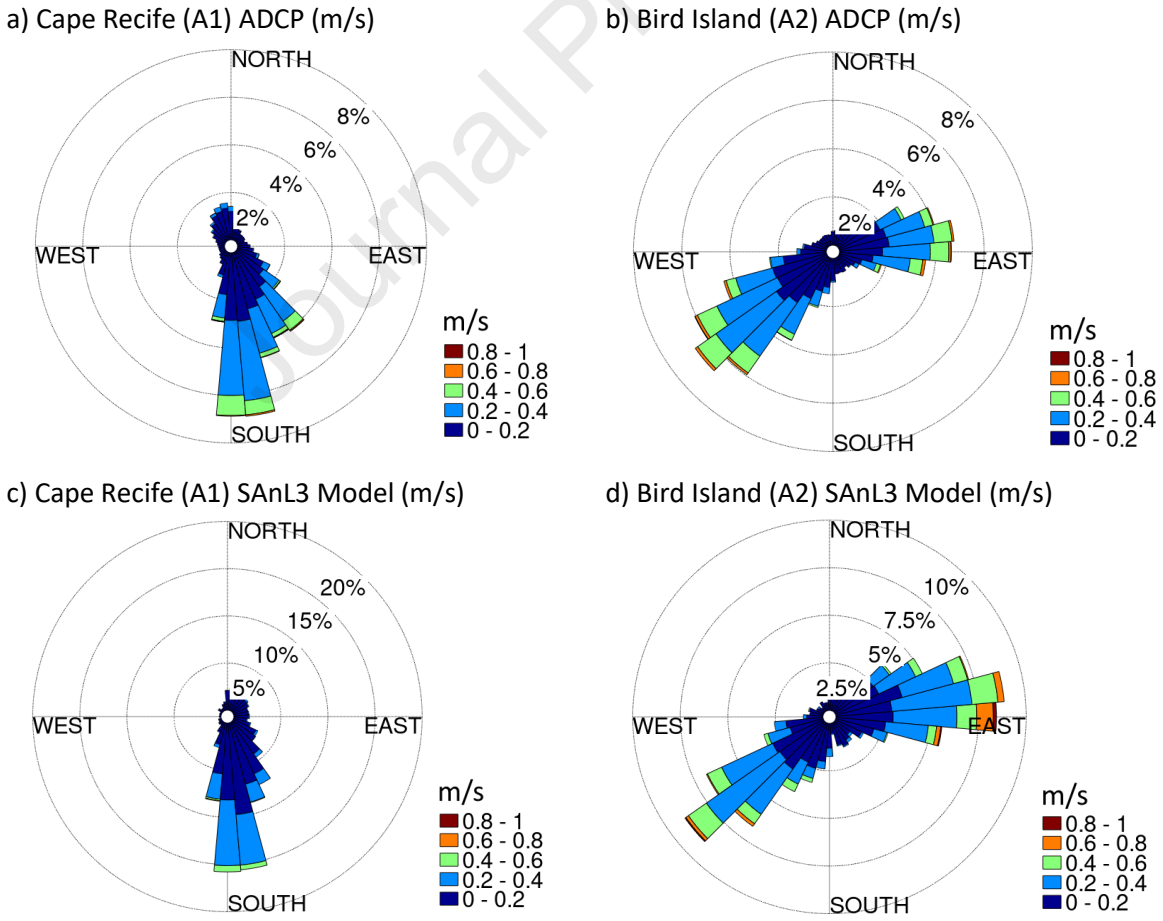

Figure 7 Depth averaged (from surface to bottom) current rose for Cape Recife (A1) and Bird Island (A2) ADCP (a,b) and SAnL3 Model in corresponding locations (c,d) from 1 January 2011 to 31 December 2015.

344

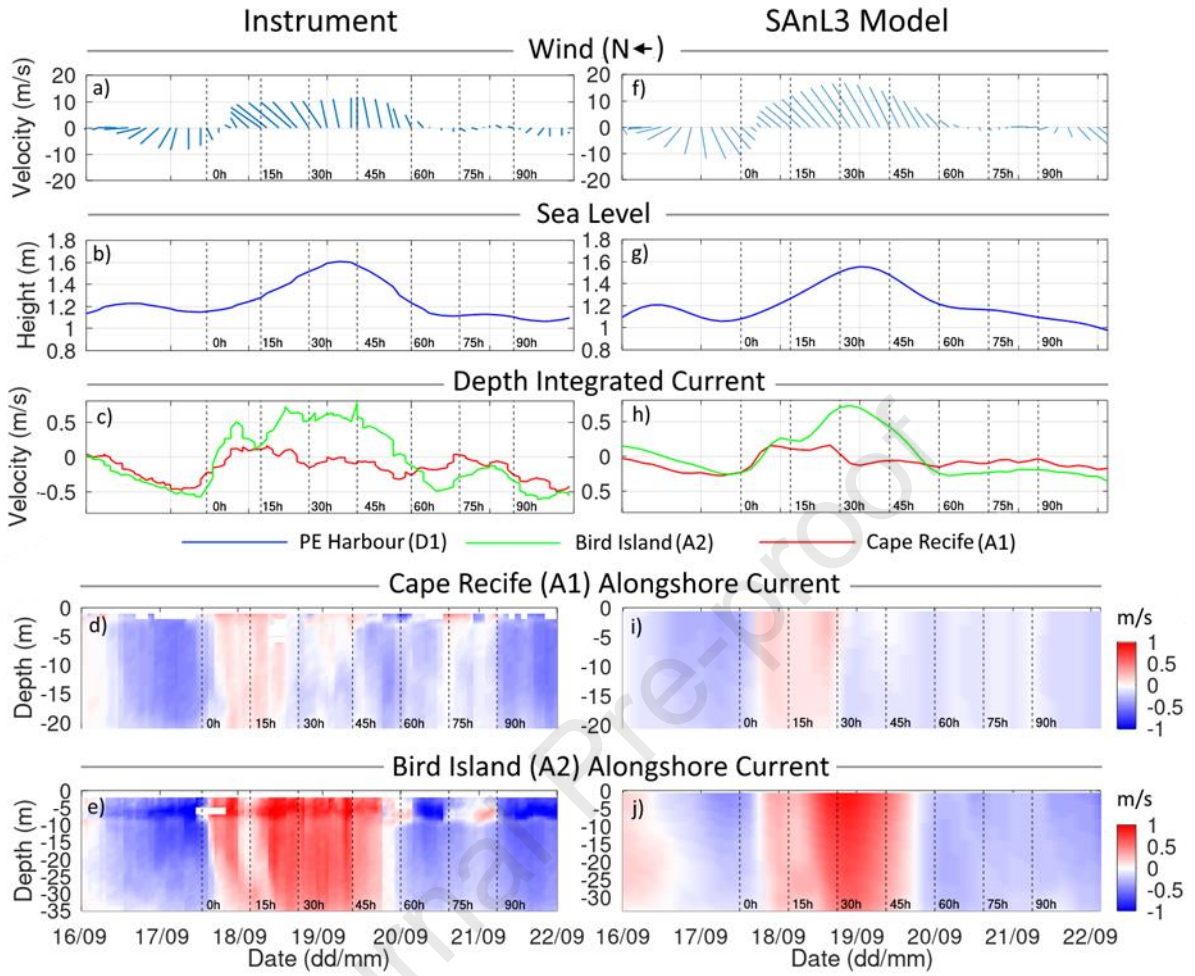

345

346 *Figure 8 The south-westerly wind event of 17 September 2014, with dashed lines showing time in 15h*
347 *increments from the onset of the event (denoted by the preceding shelf wave trough) at T0 + 0h (12h00*
348 *on 17 September 2014). Left panels (a-e) from* in situ *instrumentation, and right panels (f-j) from the*
349 *closest matching grid cell location in the numerical models. (a,f) Wind at the Port Elizabeth Airport*
350 *(Oriented northward to the left). (b,g) Sea level at the Port Elizabeth Harbour. (c,h) Depth-integrated*
351 *alongshore current at Cape Recife (A1) and Bird Island (A2). (d,i) Alongshore current at Cape Recife*
352 *and (e,j) Bird Island. Alongshore current oriented positive northward (CR (d,i)) / eastward (BI (e,j)).*

353

3.3 Examination of the event in the SAnL3 models

Within the reference model, shortly after the preceding trough at T0 + 0h (12h00 on 17 September 2014), eastward currents quickly establish after the onset of the south-westerly wind (Figure 8). Current reversals occur within approximately 3 hours of each assessment station (Figure 9b-f), with circulation in the bays switching direction from counter-clockwise to clockwise (Figure 10: T0 + 15h). This switch occurs approximately 6 hours after the start of the wave (T0 + 0h) and is evident as a reversal of the flow from southward to northward at the Cape Recife (A1) ADCP mooring (Figure 8d,i). Depth integrated current velocities peak at T0 + 30h (18h00 on 18 September 2014) (Figure 9b), with a region of very high current velocities seen over a large area south of Cape St Francis (Figure 10 left: T0 + 30h). An inverse relationship between the amplitude of the wave and the strength of the current reversals is evident (Table 4). The smallest wave height and strongest currents occur off Cape St Francis (B1), with the wave amplitude increasing as it passes offshore of Cape Recife (B2), Bird Island (B3) and Port Alfred (B4). This coincides with a progressive decline in peak wind speed at each station. Peak current velocities progressively decrease as the wave travels to the east, although the duration of each current reversal event is similar. The circulation in the two bays switches back to counter-clockwise very shortly after the peak of the wave at T0 + 30h, which was captured at the Cape Recife (A1) ADCP mooring as a current reversal back to southward flow (Figure 8d,i). Nearshore current velocities begin to decrease steadily after T0 + 45h as surface winds slow and the wave begins to move out of the domain, although strong north-eastward flows are still present over the deeper portions of the shelf south of Cape St Francis and Cape Recife (Figure 10 left: T0 + 45h). The counter-clockwise circulation patterns in St Francis and Algoa Bay become firmly established, with the near-shore currents having returned to south-westward flows (Figure 9b-f) and residual north-eastward flows in the offshore shelf areas as the domain enters the post-CTW state at midnight on 20 September 2014 (Figure 10 left: T0 + 60h).

An examination of the circulation in the SAnL3 no-wind model during the passage of the CTW reveals surprisingly similar patterns to the SAnL3 reference model (Figure 10, Figure 9). The wave progressively loses amplitude more rapidly as it travels to the north-east compared to the reference model (Table 4, Figure 9m). At Port Alfred (B4),

386 located past a sudden decrease in the continental shelf width to the east of Algoa Bay,
387 the CTW amplitude increases with a slightly greater lag in the wave peak compared
388 to the other stations. Currents are generally weaker in the no-wind model, given the
389 absence of surface wind stress, with the flow over the shelf driven by the bulk
390 displacement of water as the CTW passes. Peak current velocities become
391 progressively weaker to the east, with the average barotropic velocity 18% less than
392 the reference model (Table 4, Figure 9n). This indicates that the water displacement
393 caused by the CTW itself contributes significantly to the net flow observed during the
394 strong south-westerly wind event. In the no-wind model, a relatively well defined but
395 short-lived anticyclonic eddy forms in the lee of Cape Recife in Algoa Bay shortly after
396 the peak of the CTW (Figure 10 right: T0 + 45h and T0 + 60h). This eddy is not as well
397 defined in the reference model, instead a more general broad anticyclonic flow
398 establishes throughout the bay (Figure 10 left: T0 + 45h and T0 + 60h).

399 *3.4 Effect on along-shelf transport*

400 The along-shelf volume transport measured across the transect C1 between Cape
401 Recife and the shelf break (Figure 2) during the event is shown in Figure 11. During
402 the passage of the CTW, the flow reached a peak of 3.54Sv (2.92Sv) in the reference
403 (no-wind) model. When the balance of the volume displacement over the entire period
404 of the wave is computed across this transect, measured from T0 + 0h to the end of the
405 proceeding trough of the wave at T0 + 90h, a considerable nett displacement to the
406 east is recorded, measuring 153.3 km^3. The no-wind model also exhibits a nett volume
407 displacement to the east, measuring 93km^3 or 61% of the water volume displacement
408 in the reference model.

409

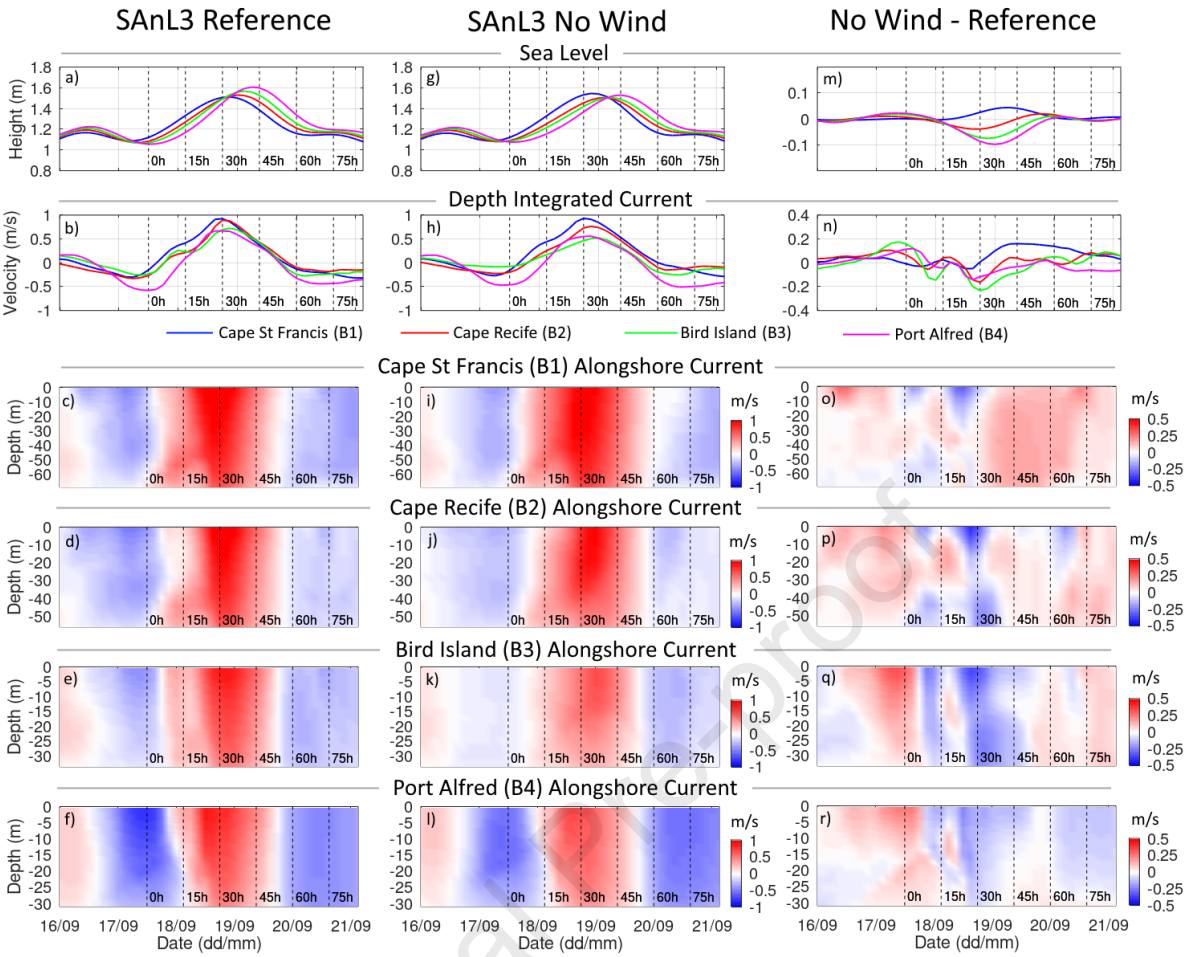

410

411 *Figure 9 Sea level, depth integrated current, and alongshore currents from 17 September 2014 to 21*
412 *September 2014 from stations B1, B2, B3, and B4 (see Figure 2) in the SAnL3 reference model (a-f),*
413 *SAnL3 no wind model (g-l), and the difference between the no wind model and the reference model (m-*
414 *r). Alongshore current oriented positive eastward/northward.*

415 *Table 4 Peak wind speed (CFSv2), wave height, and depth-integrated eastward/north-eastward*
416 *alongshore current velocity at stations B1, B2, B3, and B4 for the reference and no wind SAnL3 models.*

	Cape St Francis (B1)		Cape Recife (B2)		Bird Island (B3)		Port Alfred (B4)	
Depth	65m		55m		35m		30m	
	Wind	No Wind	Wind	No Wind	Wind	No Wind	Wind	No Wind
Wind Max	20.3m/s	--	18.8m/s	--	15.8m/s	--	13.4m/s	--
CTW Height	1.51m	1.54m	1.53m	1.5m	1.57m	1.5m	1.61m	1.53m
Alongshore Current	0.92m/s	0.93m/s	0.89m/s	0.77m/s	0.72m/s	0.53m/s	0.67m/s	0.56m/s

417

418

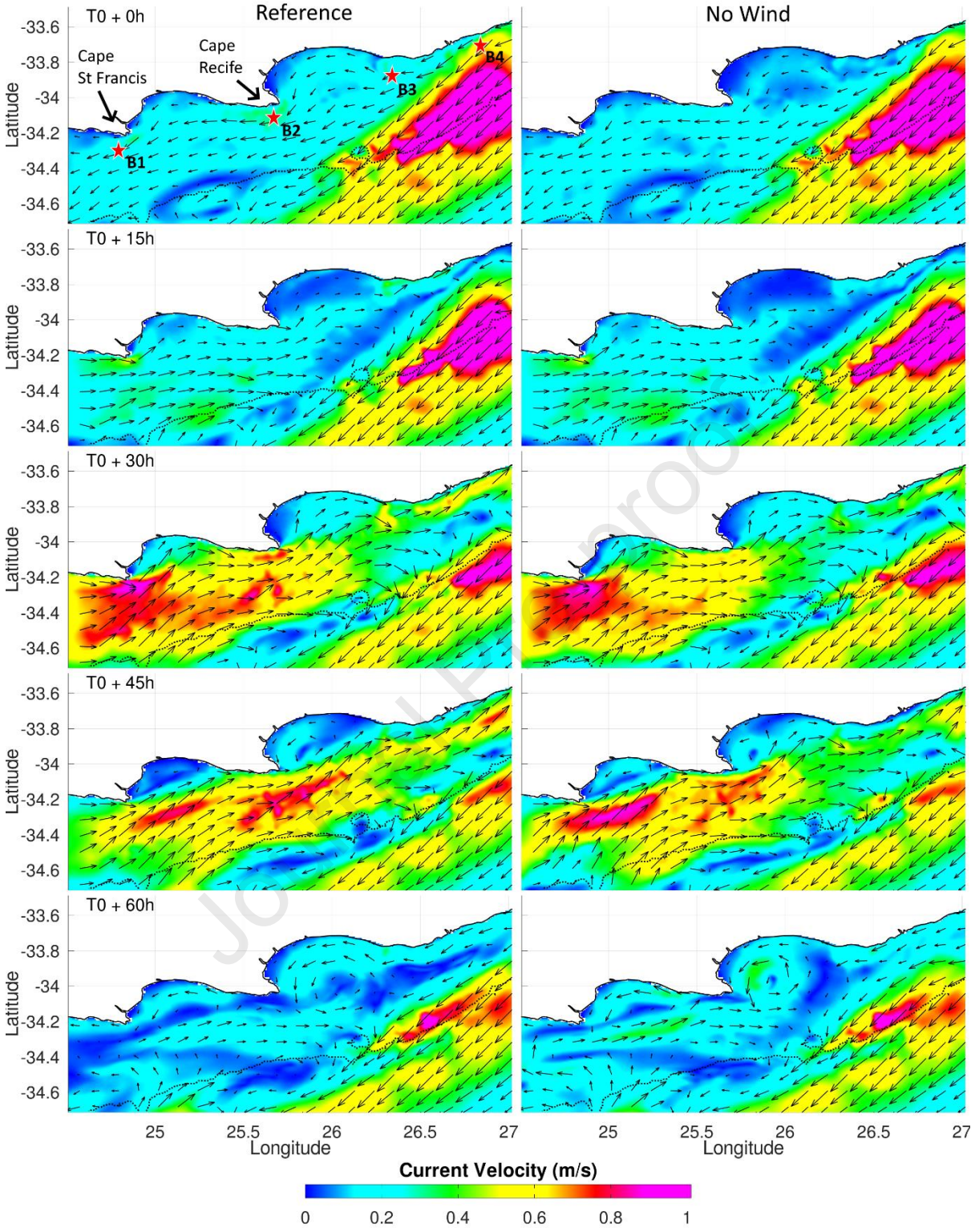

Figure 10 Depth-integrated current direction (vectors) and velocity (shading) during the passage of the coastal trapped wave in the SAnL3 reference (left) and no wind (right) model. T0 = 12h00, 17 September 2014. Dotted black line denotes the 200m isobath. B1,B2,B3, and B4 current assessment stations as per figure 2 shown top left.

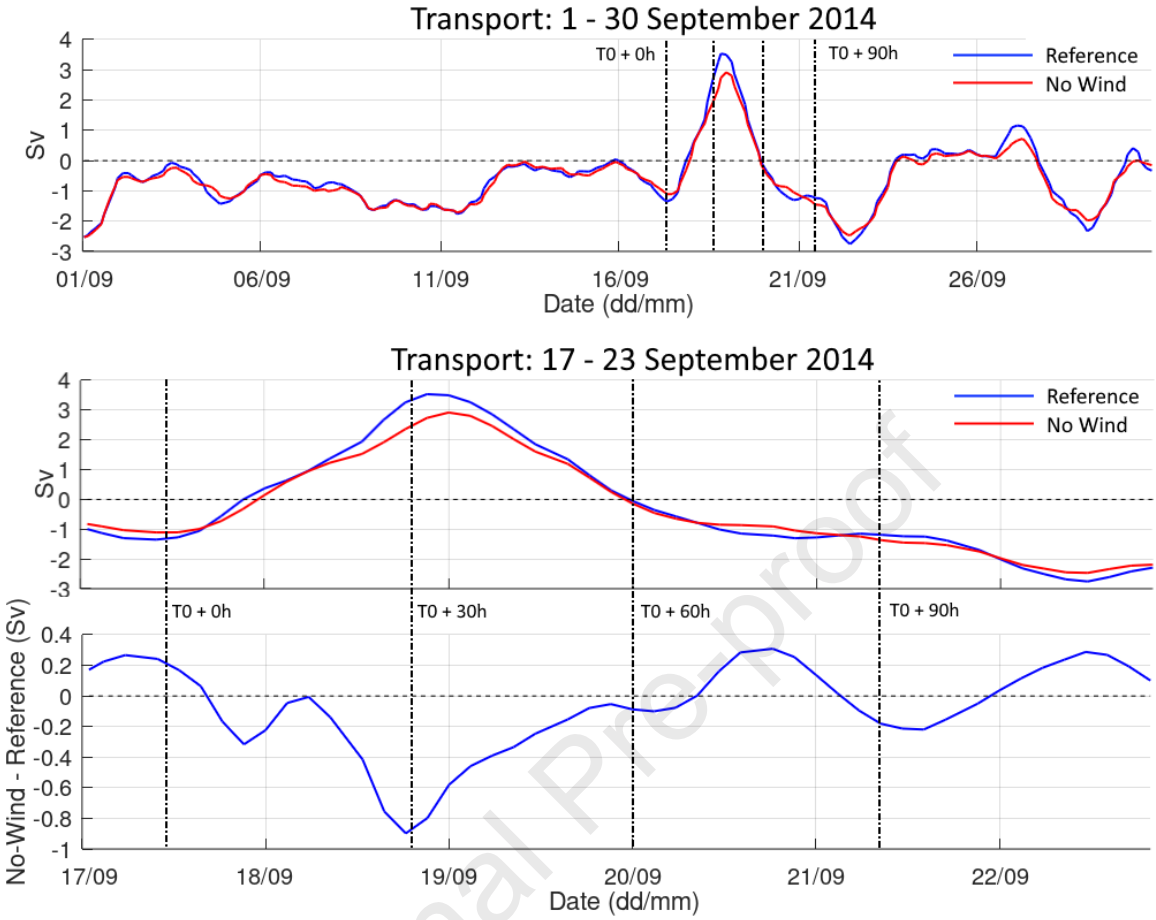

Figure 11 Along-shelf volume transport for the month of September 2014 (top) and during the passage of the CTW (middle) with the difference between the runs shown at the bottom, measured across transect C1 between Cape Recife and 10km from the inshore front of the AC in the SAnL3 reference (blue) and no-wind (red) models.

4. Discussion

A protracted south-westerly wind event lasting in approximately 45h and reaching a peak hourly average of 15.7m/s of occurred between 17 September 2014 and 20 September 2014, with a substantial response in sea level and circulation patterns captured by *in situ* sea level and ADCP instrument moorings within Algoa Bay. A dx ~1km ROMS numerical model, forced on the surface using hourly CFSv2 wind data, was able to reproduce the characteristics of the ocean response.

The prevailing south-westerly wind blowing in an approximately along-shelf direction, would be expected to result in onshore Ekman transport and subsequent sea-level set-up near the coastal boundary (Lentz and Fewings 2012). However, when considered against pressure corrected tide level records from stations to the west, it is evident that this response is also governed by the passage of lowest mode CTW, the characteristics of which were similar to that described by Goschen et al. (2012) after capturing a CTW of similar magnitude at their study site off Bird Island on 3 February 2009. Within the reference model, the peak amplitude of the CTW increases despite a decrease in wind speeds as it travels eastward (Table 4, Figure 9a). It is noted, however, that the depth of the stations gradually decreases toward the east, which would affect the wave height accordingly. Within the no-wind model the shelf wave height remains relatively similar across all stations (B1 to B4). The shelf width progressively narrows toward the east, and a similar effect of shelf width on increasing CTW amplitude and decreasing propagation speed, as observed by Kitade & Matsuyama (2000) along the southeast coast of Honshu, Japan, and demonstrated by Maiwa et al. (2010) in a shelf modelling experiment around Tasmania and the eastern coast of Australia, would be expected.

The omission of local wind forcing in the no-wind model demonstrates that remote forcing can be a significant contributor to local circulation, particularly during strong wind events. This is predominantly governed by the passing CTW, and similar processes have been investigated and described both locally (e.g, Jury et al. (1990), Schumann and Brink (1990)) and elsewhere (e.g., South-eastern Australian Coast (Church et al. 1986), Gulf of Mexico (Rivas 2017), South-west African coast (Junker et al. 2019), Fukushima coast (Kubota et al. 1981), South China Sea northern coast (Ding et al. 2012), West coast of India (Amol et al. 2012, 2018), Northern portion of

the California Current System (Engida et al. 2016)). Apart from the Port Alfred (B4) station, full depth alongshore current reversals were recorded at all other SAnL3 model stations within two model time step (6 hours) of the change in wind direction (Figure 9), with the ADCP's showing a strong full depth current reversal with a time lag of less than 4 hours to the wind switch (Figure 8). In an idealized sense, at this latitude (34° South) the establishment of the Ekman layer to its full depth would be expected to take approximately 10 hours (Gill 1982, Brink 1983). Goschen et al. (2012) found a 2.5-hour phase lag between winds and surface currents at the Bird Island (A2) DCP mooring, outside of any CTW activity. Sharp barotropic current reversals during the passage of CTW along the south coast were also noted by Schumann and Brink (1990). In case studies by Jury et al. (1990), it was found that the phase relationship between propagating wind systems and shelf waves along the west and south coast of South Africa was close, and that current reversals were primarily controlled by shelf waves which are in turn forced in phase with the propagation of alongshore winds associated with coastal lows. The currents induced by this resonance response contributes to the transient along-shelf transport of shelf waters during such events, as seen in the SAnL3 model shown in Figure 11. Comparison between the wind and no wind model across the C1 transect off Cape Recife suggests that an estimated 82% of this transient eastward transport at the peak of the event (T0 + 30h), and 61% of the total eastward movement of the water mass over the entire period of the CTW (T0 + 0h to T0 + 90h), is due primarily to remote wind forcing.

In the no-wind model, a short lived anticyclonic rotating feature forms in the lee of Cape Recife in Algoa Bay shortly after the peak of the CTW (Figure 10 right: T0 + 45h and T0 + 60h), in contrast to the reference model, where instead a broad anticyclonic flow throughout the bay establishes (Figure 10 left: T0 + 45h and T0 + 60h). Zamudio et al. (2007) investigated a similar process occurring in the Cabo Corrientes – María Islands off the Mexican West Coast. Here, it was shown that poleward moving CTW would intensify local wind forced currents and trigger the generation of anticyclonic eddies off cape-like features. While there is no published evidence to support the notion of submesoscale anticyclonic eddy formation off the lee of Cape Recife specifically, given the sharpness and orientation of the cape to the prevailing currents during the event it certainly presents itself as a strong possibility (see Røed 1980, Klinger 1994, Pichevin and Nof 1996, Cenedese and Whitehead 2000, Elkin and

Zatsepin 2013). Eddies would be expected to lose kinetic energy and vorticity due to shear from down-front wind stress (Thomas 2005, Mukherjee et al. 2016), therefore a plausible explanation as to why eddy formation off the cape is not a regularly observed feature during similar events is that the strong south-westerly winds hinder its establishment, instead spreading out into broader anticyclonic gyre-like flow throughout the bay. The curious prospect that free travelling CTW may occasionally induce eddy formation off the capes should they pass during calm wind conditions, is certainly a subject deserving further study.

5. Conclusion

In situ instruments and high resolution ROMS model data were used to investigate the effects of an eastward travelling wind system on sea level and circulation responses in the shelf and bays on the eastern Agulhas Bank. Measurements at tide level recorders across the western and southern coasts of South Africa indicated the event was associated with an eastward travelling CTW that passed through the study region. Sudden alongshore current reversals to the full depth were seen at the ADCP sites to the south-west of Bird Island and to the east of Cape Recife, with the ROMS model showing this current reversal also occurring south of Cape St Francis and south of Cape Recife, with particularly strong currents developing here at the peak of the CTW (>1 m/s). The omission of local wind forcing in the model demonstrated that remote forcing can be a significant contributor to local circulation, particularly during strong wind events. An along-shelf transport assessment over a cross-shelf transect south of Cape Recife illustrated that remote wind forcing can be responsible for an estimated 61% of the total eastward movement of the water mass over the entire period of the event. Curiously, when wind was removed in the model, a short-lived anticyclonic eddy-like rotating feature formed in the eastern lee of Cape Recife in Algoa Bay shortly after the peak of the CTW, in contrast to the broad anticyclonic flow that typically establishes throughout the bay seen in the reference model run.

The substantial along-shelf movement of water coupled with the changes in circulation patterns within the bays highlight the importance of such wind events on governing water exchange between the bays and the shelf. This has significant implications for regional marine biota, and the effects of climate change on local pressure and wind

systems could indeed alter the characteristics of these marine environments by enhancing or diminishing the movement and exchange of shelf waters.

6. Acknowledgements

We are grateful to the South African Weather Service (SAWS), the South African Environmental Observation Network's (SAEON) Elwandle Node, and the South African National Hydrographers Office (SANHO) for providing the invaluable weather, ocean sensor, and tide gauge data respectively for this study.

7. References

Amol P, Shankar D, Aparna SG, Shenoi SSC, Fernando V, Shetye SR, Mukherjee A, Agarvadekar Y, Khalap S, Satelkar NP 2012. Observational evidence from direct current measurements for propagation of remotely forced waves on the shelf off the west coast of India. *Journal of Geophysical Research: Oceans* 117: 1–15.

Amol P, Vijith V, Fernando V, Pednakar P, Singh J 2018. Impact of local and remote winds on the shelf circulation off the central west coast of India. *Ocean Dynamics* 68: 1607–1623.

Bailey D 2020. *Ocean Dynamics of the Shelf and Bays of the Eastern Agulhas Bank: A Process-Oriented Numerical Modelling Study*. Nelson Mandela University.

Beal LM, Elipot S, Houk A, Leber GM 2015. Capturing the Transport Variability of a Western Boundary Jet: Results from the Agulhas Current Time-Series Experiment (ACT)*. *Journal of Physical Oceanography* 45: 1302–1324.

Bremner J 1983. Properties of logarithmic spiral beaches with particular reference to Algoa Bay. *Sandy beaches as ecosystems*.

Brink KH 1983. The near-surface dynamics of coastal upwelling. *Progress in Oceanography* 12: 223–257.

Brink KH 1990. On the Damping of Free Coastal-Trapped Waves. *Journal of Physical Oceanography* 20: 1219–1225.

Brink KH 1991. Coastal-Trapped Waves and Wind-Driven Currents over the Continental Shelf. *Annual Review of Fluid Mechanics* 23: 389–412.

Brink KH 2006. Coastal Trapped Waves with Finite Bottom Friction. 2005: 2–3.

Cenedese C, Whitehead JA 2000. Eddy shedding from a boundary current around a cape over a sloping bottom. *Journal of Physical Oceanography* 30: 1514–1531.

Church JA, Freeland HJ, Smith RL 1986. Coastal-trapped waves on the East Australian continental shelf part I: Propagation of modes. *Journal of Physical Oceanography* 16: 1929–1943.

Cucco A, Quattrocchi G, Zecchetto S 2019. The role of temporal resolution in modeling the wind induced sea surface transport in coastal seas. *Journal of Marine Systems* 193: 46–58.

Ding Y, Bao X, Shi M 2012. Characteristics of coastal trapped waves along the northern coast of the south china sea during year 1990. *Ocean Dynamics* 62: 1259–1285.

Elkin DN, Zatsepin AG 2013. Laboratory investigation of the mechanism of the periodic eddy formation behind capes in a coastal sea. *Oceanology* 53: 24–35.

Engida Z, Monahan A, Ianson D, Thomson RE 2016. Remote forcing of subsurface currents and temperatures near the northern limit of the California Current System. *Journal of Geophysical Research: Oceans* 121: 7244–7262.

Gaspar P, Ponte RM 1997. Relation between sea level and barometric pressure determined from altimeter data and model simulations. *Journal of Geophysical Research C: Oceans* 102: 961–971.

Gill AE 1982. *Atmosphere-Ocean Dynamics* (1st Editio edn). Academic Press.

Gill AE, Schumann EH 1974. The Generation of Long Shelf Waves By the Wind. *Journal of Physical Oceanography* 4: 83–90.

Goschen W, Schumann E, Bernard K, Bailey S, Deyzel S 2012. Upwelling and ocean structures off Algoa Bay and the south-east coast of South Africa. *African Journal of Marine Science* 37–41.

Goschen WSW, Schumann EH 1988. Ocean current and temperature structures in Algoa Bay and beyond in November 1986. *South African Journal of Marine Science* 7: 101–116.

Haidvogel DB, Beckmann A 1999. *Numerical Ocean Modelling*. Imperial College Press.

Holt JT, Allen JI, Proctor R, Gilbert F 2005. Error quantification of a high-resolution coupled hydrodynamic-ecosystem coastal-ocean model: Part 1 model overview and assessment of the hydrodynamics. *Journal of Marine Systems* 57: 167–188.

Junker T, Mohrholz V, Schmidt M, Siegfried L, van der Plas A 2019. Coastal trapped wave propagation along the southwest African shelf as revealed by moored observations. *Journal of Physical Oceanography* 49: 851–866.

Jury M, MacArthur C, Reason C 1990. Observations of trapped waves in the atmosphere and ocean along the coast of Southern Africa. *South African Geographical Journal* 72: 33–46.

Kitade Y, Matsuyama M 2000. Coastal trapped waves with several day period caused by wind along the southeast coast of Honshu, Japan. *Journal of Oceanography* 56: 727–744.

Klinger BA 1994. Baroclinic eddy generation at a sharp corner in a rotating system. *Journal of Geophysical Research* 99.

Krug M, Swart S, Gula J 2017. Submesoscale cyclones in the Agulhas current. *Geophysical Research Letters* 44: 346–354.

Kubota M, Nakata K, Nakamura Y 1981. Continental shelf waves off the fukushima coast Part I: Observations. *Journal of the Oceanographical Society of Japan* 37: 267–278.

Lentz SJ, Fewings MR 2012. The wind- and wave-driven inner-shelf circulation. *Annual Review of Marine Science* 4: 317–343.

Lutjeharms JRE, Roberts HR 1988. The Natal Pulse: An Extreme Transient on the Agulhas Current. *Journal of Geophysical Research* 93: 631–645.

Lutjeharms JRE, Boebel O, Rossby HT 2003a. Agulhas cyclones. *Deep Sea Research Part II: Topical Studies in Oceanography* 50: 13–34.

Lutjeharms JRE, Catzel R, Valentine HR 1989. Eddies and other boundary phenomena of the Agulhas Current. *Continental Shelf Research* 9: 597–616.

Lutjeharms JRE, Penven P, Roy C 2003b. Modelling the shear edge eddies of the southern Agulhas Current. *Continental Shelf Research* 23: 1099–1115.

Maiwa K, Masumoto Y, Yamagata T 2010. Characteristics of coastal trapped waves along the southern and eastern coasts of Australia. *Journal of Oceanography* 66: 243–258.

Marchesiello P, Debreu L, Couvelard X 2009. Spurious diapycnal mixing in terrain-following coordinate models: The problem and a solution. *Ocean Modelling* 26: 156–169.

Marchesiello P, Mcwilliams JC, Shchepetkin A 2001. Open boundary conditions for long-term integration of regional oceanic models. *Ocean Modelling* 3: 1–20.

Mason E, Molemaker J, Shchepetkin AF, Colas F, McWilliams JC, Sangrà P 2010. Procedures for offline grid nesting in regional ocean models. *Ocean Modelling* 35: 1–15.

Mukherjee S, Ramachandran S, Tandon A, Mahadevan A 2016. Production and destruction of eddy

kinetic energy in forced submesoscale eddy-resolving simulations. *Ocean Modelling* 105: 1339–1351.

Pattrick P, Strydom N, Goschen W 2013. Shallow-water, nearshore current dynamics in Algoa Bay, South Africa, with notes on the implications for larval fish dispersal. *African Journal of Marine Science* 35: 269–282.

Penven P, Chang N, Shillington F 2006a. Modelling the Agulhas Current using SAfE (Southern Africa Experiment). *Geophysical Research Abstracts* 8.

Penven P, Debreu L, Marchesiello P, McWilliams JC 2006b. Evaluation and application of the ROMS 1-way embedding procedure to the central california upwelling system. *Ocean Modelling* 12: 157–187.

Pichevin T, Nof D 1996. The eddy cannon. *Deep Sea Research Part I: Oceanographic Research Papers* 43: 1475–1507.

Rivas D 2017. Wind-driven coastal-trapped waves off southern Tamaulipas and northern Veracruz, western Gulf of Mexico, during winter 2012–2013. *Estuarine, Coastal and Shelf Science* 185: 1–10.

Roberts MJ 2010. Coastal currents and temperatures along the eastern region of Algoa Bay, South Africa, with implications for transport and shelf-bay water exchange. *African Journal of Marine Science* 32: 145–161.

Roberts MJ, van der Lingen CD, Whittle C, van den Berg M 2010. Shelf currents, lee-trapped and transient eddies on the inshore boundary of the Agulhas Current, South Africa: their relevance to the KwaZulu-Natal sardine run. *African Journal of Marine Science* 32: 423–447.

Røed LP 1980. Curvature effects on hydraulically driven inertial boundary currents. *Journal of Fluid Mechanics* 96: 395–412.

Saha S, Moorthi S, Wu X, Wang J, Nadiga S, Tripp P, Behringer D, Hou YT, Chuang HY, Iredell M, et al. 2014. The NCEP climate forecast system version 2. *Journal of Climate* 27: 2185–2208.

Schumann EH 1983. Long-period coastal trapped waves off the southeast coast of Southern Africa. *Continental Shelf Research* 2: 97–107.

Schumann EH 1999. Wind-driven mixed layer and coastal upwelling processes off the south coast of South Africa. *Journal of Marine Research* 57: 671–691.

Schumann EH 2013. Sea level variability in South African estuaries. *South African Journal of Science* 109: 1–7.

Schumann EH, Brink KH 1990. Coastal-trapped waves off the coast of South Africa: Generation, propagation and current structure. *Journal of Physical Oceanography* 20: 1206–1218.

Schumann EH, van Heerden I 1988. Observations of Agulhas Current frontal features south of Africa, October 1983. *Deep Sea Research Part A, Oceanographic Research Papers* 35: 1355–1362.

Schumann EH, Churchill JRS, Zaayman HJ 2005. Oceanic variability in the western sector of Algoa Bay , South Africa. *African Journal of Marine Science* 27: 65–80.

Shchepetkin AF, McWilliams JC 2005. The regional oceanic modeling system (ROMS): a split-explicit, free-surface, topography-following-coordinate oceanic model. *Ocean Modelling* 9: 347–404.

Swart VP, Largier JL 1987. Thermal structure of Agulhas Bank water. *South African Journal of Marine Science* 5: 243–252.

Tedesco P, Gula J, Ménesguen C, Penven P, Krug M 2019. Generation of Submesoscale Frontal Eddies in the Agulhas Current. *Journal of Geophysical Research: Oceans* 124: 7606–7625.

Thomas LN 2005. Destruction of potential vorticity by winds. *Journal of Physical Oceanography* 35: 2457–2466.

Tilney RL, Nelson G, Radloff SE, Buxton CD 1996. Ichthyoplankton distribution and dispersal in the Tsitsikamma National Park marine reserve, South Africa. *South African Journal of Marine Science* 17: 1–14.

Zamudio L, Hurlburt HE, Metzger EJ, Tilburg CE 2007. Tropical wave-induced oceanic eddies at Cabo Corrientes and the María Islands, Mexico. *Journal of Geophysical Research: Oceans* 112: 1–17.

- The Regional Oceanographic Modelling System has predictive skill in reproducing coastal trapped wave events along the south coast of South Africa
- Sudden alongshore current reversals are seen to full depth in the model and ADCP mooring data
- The model shows very strong eastward currents develop off Cape St Francis and Cape Recife
- The model shows very large volume displacement caused by the CTW, which carries most of the energy from remote wind forcing to the west of Oyster Bay

Declaration of interests

☐ The authors declare that they have no known competing financial interests or personal relationships that could have appeared to influence the work reported in this paper.

☒ The authors declare the following financial interests/personal relationships which may be considered as potential competing interests:

Dylan F. Bailey reports a relationship with Bayworld Museum Complex that includes: employment.